Mechanical characterization and numerical modeling of TPMS lattice structures subjected to impact loading

Rafael Santiago[1], Sarah Almahri[1], Dong-Wook Lee[1], Haleimah Alabdouli[1], Omar Banabila[1], Henrique Ramos[1,2], Mohammed Alteneiji[1], Zhongwei Guan[1], and Marcilio Alves[2]*

[1]Technology Innovation Institute, Advanced Materials Research Centre, Abu Dhabi, United Arabic Emirates.
[2]Department of Mechatronics and Mechanical Systems Engineering, Group of Solid Mechanics and Structural Impact, University of São Paulo (USP), Brazil.

Abstract. The advent of Powder Bed Fusion (PBF) techniques allows the additive manufacturing of complex structures, as Triply Periodic Minimal Surfaces (TPMS) lattices, which exhibit promising characteristics for impact applications, such as lightweight and high-energy absorption. Thus, this work aims to develop a numerical model of TPMS structures to investigate the mechanical response of such structures when subjected to impact loadings. To fulfill this task, stainless steel samples made by PBF technique were mechanically characterized at different strain rates using a universal testing machine and Split Hopkinson Pressure Bar. The testing campaign also explored the compressive and tensile material response, with the strain field being monitored by Digital Image Correlation technique. It was noted that the material exhibits a similar elasto-plastic response on both tension and compression and an evident strain rate hardening when the material is loaded from static (0.001 s^{-1}) to dynamic strain rates (4000 s^{-1}). Constitutive parameters were then obtained and implemented in an explicit finite element model developed through Abaqus CAE. Samples of TMPS lattices were manufactured and tested at different loading velocities, which showed that the FE model developed can be used to predict the impact response of TMPS lattices.

1 Introduction

The lightweight structures subject to impact loading are widely used in automotive, aerospace, military, railway, and naval application, such as wing edge, impact absorbers, helmets, armoring, and others. The advent of Additive Manufacturing (AM) techniques broadens the use of cellular materials once complex structures could be efficiently designed and manufactured, highlighting applications of lattice structures [1-2]. With this given, the Triple Minimal Periodic Surfaces (TPMS) lattices are a promising stretching-dominated

* Corresponding author: rafael.santiago@tii.ae .

lightweight lattice for higher energy absorption, highlighted by the scientific community. The TPMS presents a self-structured shell architecture suitable for powder-bed fusion AM technique that can be up to two times stiffer than truss-based lattices [3-4].
The TPMS reduces the stress concentration exhibit a smoother crush behavior when compressed compared to truss-based lattices [5-10]. Al-Ketan et al. explored the compressive behavior of Primitive, Gyroid, Diamond, and IWP lattices under low strain rates made by AM maraging steel [9], [11]. It was reported that the layer thickness influences the surface finishing and, consecutively, the lattice mechanical properties. The heat treatment also can change the lattice toughness, energy absorption, and ductility. The authors concluded that diamond lattices exhibited superior compressive modulus and strength than the other topologies. Novak et al. [12] studied Diamond, Gyroid, IWP, and Primitive TPMS structures at different relative densities under strain rates up to 14.2 /s. This study pointed to an increase in plateau stress and specific energy absorption, with no systematic trend at the velocity studied.
Split Hopkinson Pressure Bars (SHPB) have been used for characterizing bulk material under tension, compression, and shear loadings [13]–[15]. Kariem et al. [15] explored the SHBP techniques, conducting a round-Robin test between four research centers for characterizing aluminum, copper, stainless steel, and low-carbon steel alloys. This effort showed consistent results from the laboratories involved, highlighting the robustness of the techniques for obtaining the response of materials under high strain rates.
This work presents the mechanical characterization of 316L stainless steel at strain rates from 0.001/s up to 4000/s. This alloy is manufactured by additive manufacturing and is also used to produce TPMS lattices. The material constitutive parameters were defined and used in an explicit finite element (FE) model to represent the TPMS impact response. The FE was compared to experimental data, showing that it could predict the response of the lattice. The FE was also evaluated with complex lattices architectures, capturing the lattice mechanical response influence due to changes in the lattice pattern.

2 Materials

The TPMS structures were made of 316L stainless steel, Table 1, additively manufactured by Selective Laser Melting (SLM) technique. The SLM equipment used was an EOS M290 metal 3d printer (GmbH, Munich, Germany) with a 350 W laser power output, set the platform temperature as 160 °C and 40 μm layer thickness. The material was then heat-treated for 2 hours at 600°C to promote stress relief from manufacturing.
Tensile and compressive testing specimens were made by the same material and process described above to keep the material loading direction parallel to the build chamber base. The samples were extracted from the build chamber by localized grinding, and no machining processes were performed.

Table 1. Chemical compositions of atomized 316 stainless steel powder.

Chemical composition (wt%)								
C	Si	Mn	Cr	Ni	Mo	S	P	Fe
≤0.03	≤1	≤2	16-18	10-12	2-3	≤0.045	≤0.03	Balance

Schwarz-diamond (SD) TPMS lattices [8] were used to validate the numerical model, which topology is defined by Eq. 1. The testing samples were made of 4 x 4 x 4 unit cells forming a 16mm x 16mm x 16mm cube at three different relative densities ($\rho_{rel}, Eq. 2$) according to

the wall thickness chosen. The samples were previously tested at static (0.005/s) and dynamic (2057/s) strain rates, which data was compared to FE results.

$$\cos(x)\cos(y)\cos(z) - \sin(x)\sin(y)\sin(z)(x) = c \quad (1)$$

$$\rho_{rel} = \frac{\rho_{lattices}}{\rho_{material}} \quad (2)$$

3 Methods

3.1 Mechanical Characterization

The quasi-static mechanical tensile/compression tests were conducted in a universal testing machine (UTM) Instron 3369 with a 50 KN load cell. Tensile samples based on ASTM E8 [16] standard were used, with 32 mm effective gauge length and 2 mm thickness, Figure 1a. The strain field on the specimen surface was measured up to high strain levels by using Correlated Solutions VIC-2D system, with one 5 megapixels cameras taken images at 1 fps, Figure 1b. Compressive 5mm diameter disc, with 3mm height, samples were used for compressive tests. The material true stress, σ_t, was obtained as follows

$$\sigma_t = \frac{F}{A_0}(1 + \varepsilon) \quad (3)$$

where, A_0 is the specimen initial effective cross-section, F is the uniaxial load given by UTM and ε is the uniaxial strain provided by DIC, for the tensile test; or $\varepsilon = \Delta l / l_0$ for compressive tests, with Δl and l_0 the UTM crosshead displacement and initial specimen height, respectively.

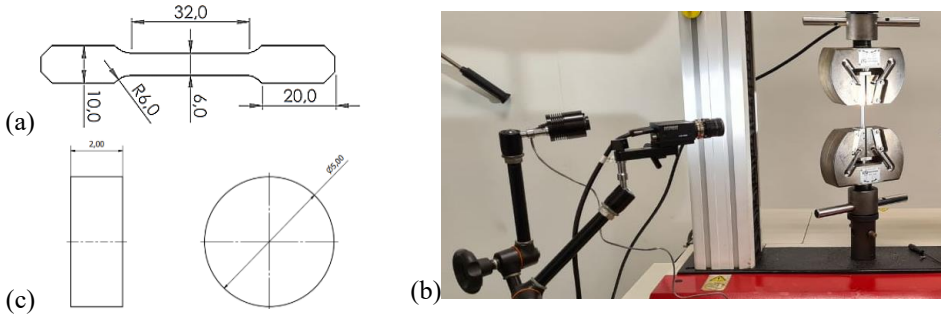

Fig. 1. (a) tensile specimen*, (b) experimental setup used and (c) compressive specimen* (* dimensions in mm).

Dynamic material characterization tests were conducted using a compressive Split Hopkinson Pressure Bar (SHPB) [15]. The compressive samples were fixed between two 2m long metallic bars, made of SAE 1055 steel bars and 25 mm diameter, Fig. 2. The test starts when a striker is pneumatically accelerated and impacts the bar, which results in an elastic pulse that travels along the incident bar, Figure 2. The pulse reaches the opposite bar end, which is partially reflected inside the bar or passes through the specimen the reaching the transmitted bar. The incident ($\varepsilon_i(t)$), transmitted ($\varepsilon_t(t)$) and reflected ($\varepsilon_r(t)$) pulses are recorded by strain gauges installed on the bars, whereby the specimen stress, strain and strain rate can be defined as:

$$\varepsilon_i(t) = \varepsilon_t(t) - \varepsilon_r(t) \quad (4)$$

$$\sigma(t) = E_B \frac{A_B}{A_0} \varepsilon_t(t) \quad (5)$$

$$\varepsilon_s(t) = -\frac{2c_0}{l_s} \int_0^t \varepsilon_r(t) dt \quad (6)$$

$$\dot{\varepsilon}_s(t) = -\frac{2c_0}{l_s} \varepsilon_r(t) \quad (7)$$

where l_s is the specimen length, $c_0 = \sqrt{E_b/\rho_b}$ the elastic wave speed, given by elastic modulus of the bar, E_b, and density, ρ_b; while A_B is the cross-section of the bar. The tests were conducted using the same compressive specimen described previously at about 2000/s and 4000/s strain rates, being the data reduced by a subroutine in Matlab.

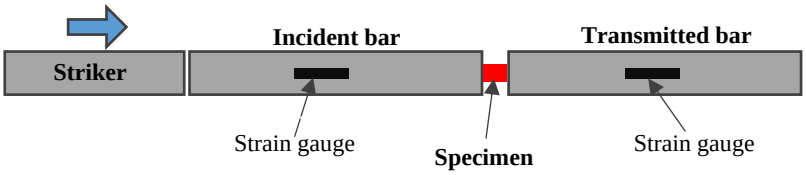

Fig. 2. The schematic diagram and components for the Split Hopkinson Pressure Bar used for dynamic tests.

3.2 Numerical modeling

An explicit FE was developed in Abaqus/Explicit code, modeling whole lattices 16mm cubes with 64 lattices unit cells and the shell thickness according to the relative density expected. The SD isosurface was implemented on Matlab software, and post-processed before be modeled in the FE software. Modified quadratic tetrahedral elements (C3D10M) were used, and the lattices cube was placed between two rigid surfaces, Figure 3. The upper surface is movable, in which the impact mass/velocity is defined, or the prescribed movement, in the case of quasi-static modeling. The lower face is fixed for all the cases, with a surface-to-surface contact law (hard contact) was defined.

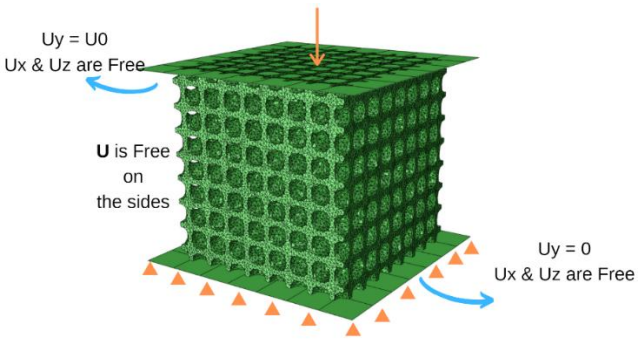

Fig. 3. Example of FE mesh and boundary conditions for the Schwarz diamond numerical model.

4 Results and Discussion

4.1 Mechanical Characterization

The tensile tests were carried using the samples described previously with three repetitions for each testing condition. All the samples presented failure within the effective gauge length, and the DIC was used to obtain the localized stain inside the gauge length, Fig. 4. The stress-strain curves for the specimens tested at quasi-static strain rates under tension and compression are shown in Figure 5; whence Young's modulus, ultimate tensile strength, fracture strain, and Poisson's ratio were extracted, Table 2. The Johnson-Cook (JC) plasticity model was used [15] for the lattice, expressed as:

$$\sigma_p = \left[A + B\varepsilon_p^n\right]\left[1 + Cln\left(\frac{\dot{\varepsilon}}{\dot{\varepsilon}_o}\right)\right] \qquad (8)$$

where σ_p is the plastic stress,ε_p is the plastic strain, and $\dot{\varepsilon}_o$ the reference strain rate. The parameters A, B, and n were also obtained from quasi-static strain-stress curves, summarized in Table 2.

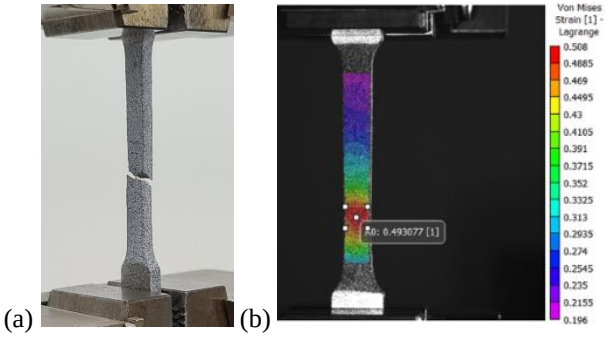

Fig. 4. Example of (a) specimen failure and (b) DIC data extraction.

The material dynamic response obtained by SHPB tests is presented in Fig. 6a for 1880/s and 3990/s strain rates. It can be noted an evident material strain hardening at velocity range tested compared to its quasi-static response. Due to the limitations of the testing setup, the tests were finished at 25% strain. The JC strain rate parameter, *C*, was extracted considering 20% of compressive strain, summarized in Table 2.

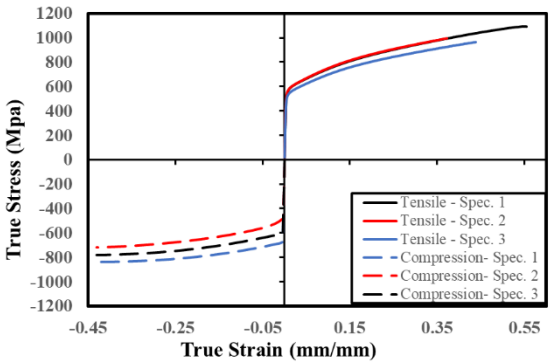

Fig. 5. Quasi-static strain-stress response of stainless steel 316L made by SLM.

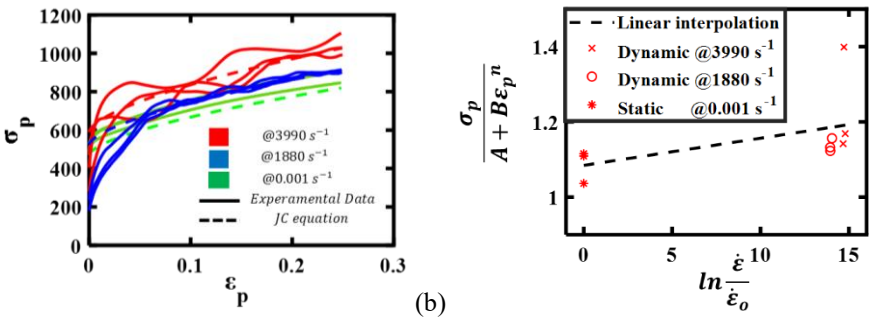

Fig. 6. Dynamic strain-stress response of stainless steel 316L made by SLM.

Table 2: Mechanical response and constitutive parameters of stainless steel 316L made by SLM.

Young's modulus, E (GPa)	**Yield Stress, σ_y (MPa)**	**Ultimate strength, σ_{UTS} (MPa)**	**Fracture Stress, σ_f (MPa)**	**Fracture strain, ε_f**
155±7	490±17	1070±47	1044±51	0.57±0.04
Poisson's ratio, ν	**A (MPa)**	**B (MPa)**	**n**	**C**
0.33±0.01	490±17	871±60	0.57±0.02	0.0072

4.2 Numerical Modelling

The SD TPMS were modeled at the relative densities of 27.1%, 34.5 %, and 44.8%, representing the average measured from the specimens experimentally tested. A mesh sensitivity analysis was performed, noting that 0.3 mm element size achieves the best compromise between processing time and result convergence. The material parameters implemented are listed in Table 2, and no material damage or failure was implemented at this stage.

Figure 7 shows the quatitative comparison of the static and dynamic response of SD with 27.1% relative density. It was noted that the FE model could predict the overall behavior observed from the lattices at both strain rates. The compression is uniformly applied on all the lattice layers through the specimen height, with a visible lateral expansion observed at high deformation levels. The FE also predicted the shear-dominated deformation mechanism, formed by diagonal shear deformations when the lattices reach the plateau stage. No evident material failure was observed from the experimental test, corroborated by the numerical model accumulated plastic deformation data.

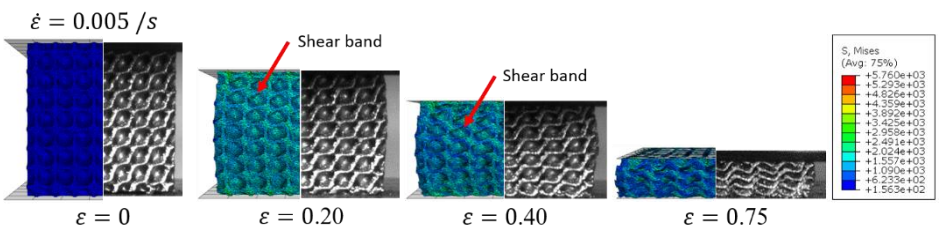

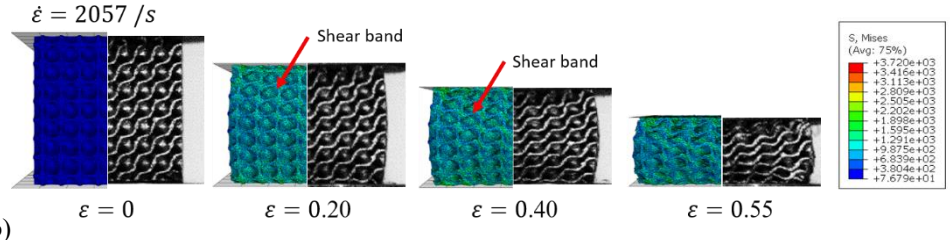

(b)

Fig. 7. Quantitative numerical and experimental results of SD TPMS (a) quasi-static and (b) dynamically loaded.

Figure 8 summarizes the strain-stress response of the SD lattice when loaded at quasi-static and dynamic strain rates. A good agreement between numerical and experimental responses was evident for all the relative densities, and the strain rate effects were also evident in the FE results. The plateau level and absorbed energy, W (Eq. 9), were extracted from the numerical and experimental strain-stress curves, being summarized in Fig. 9 and Table. 3. It was obtained an overall difference between numerical and experimental results of 5.25%, which leads to using the developed model in the range of relative densities and strain rates for the given lattice made by stainless steel 316L-SLM.

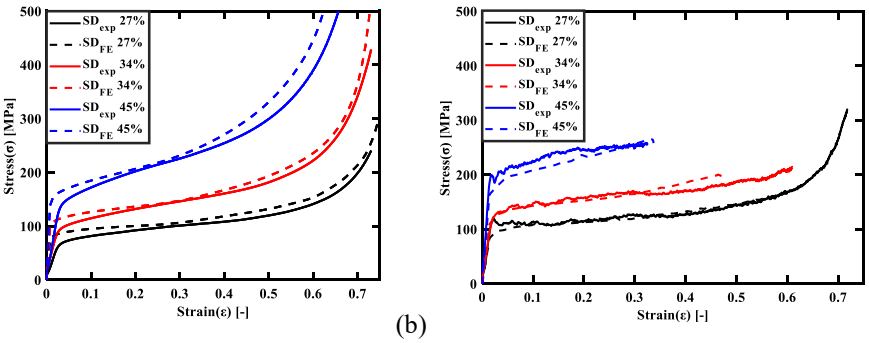

(a) (b)

Fig. 8. Strain-stress responses of SD TPMS (a) quasi-static and (b) dynamic loaded.

$$W = \int_0^{\varepsilon_u} \sigma d\varepsilon \qquad (9)$$

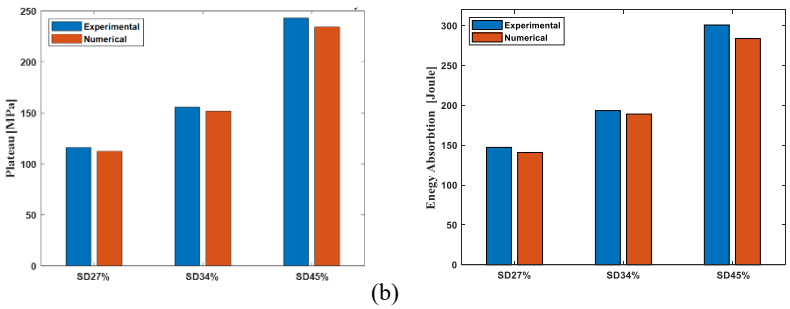

(a) (b)

Fig. 9. Numerical and experimental comparison of (a) plateau stress level and (b) impact energy absorbed by SD lattices under dynamic loadings.

Tab. 3. Summary of plateau level and energy absorbed for the SD TPMS at (a) quasi-static and (b) dynamic strain rates.

(a) Quasi-static (0.005 /s)						
ρ_{rel} (%)	Plateau level (MPa)			Energy absorbed (J)		
	Experimental	Numerical	Deviation	Experimental	Numerical	Deviation
27.1%	96.2	104.4	8.5 %	72.3	80.4	11.2 %
34.5%	138.8	143.3	3.3 %	105.4	112.0	6.2 %
44.8%	213.8	221.3	3.5 %	146.9	160.0	8.9 %

(b) Dynamic (2057 /s)						
ρ_{rel}(%)	Plateau level (MPa)			Energy absorbed (J)		
	Experimental	Numerical	Deviation	Experimental	Numerical	Deviation
27.1%	116.0	112.4	3.1%	36.0	34.4	4.3%
34.5%	155.6	151.7	2.5%	47.2	46.2	2.3%
44.8%	243.1	234.4	3.6%	73.5	69.3	5.6%

The FE model to predict the response of graded SD lattices under impact loadings, Figure 10. In this analysis, the lattices relative density changes from 10% up to 50% through height (named g-SD), keeping the same overall mass of the non-graded SD lattices with 30% relative density.

The FE could predict the response of the g-SD, which is different from the SD, once the g-SD exhibits a high deformation at the low relative density lattices, with an evident lateral expansion at this region, Figures 10a-b. Additionally, the g-SD shows a crescent mainly linear crush-band on its strain-stress response, which is different from the mainly flat plateau evident in the SD. The deformation mechanism was also changed once g-SD showed a failure of a whole horizontal layer. The energy absorbed by g-SD also tends to be larger than the absorbed by SD.

This preliminary study exemplifies the capability of the FE model developed for predicting the impact performance of complex lattices architectures.

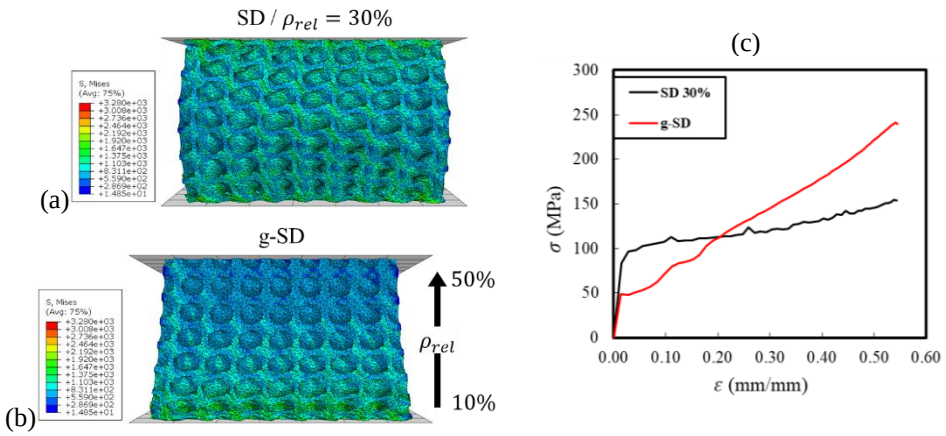

Fig. 10. Numerical prediction of a graded TMPS lattice: (a) non-graded, (b) graded and (c) strain-stress comparisons.

5 Conclusions

This study described the mechanical characterization and numerical modeling of Schwarz-diamond TPMS lattices structures made by stainless steel 316L via additive manufacturing.

The static and dynamic response of the material was obtained through Universal Testing Machine and a Split Hopkinson Pressure Bar, which input in an explicit finite element able to predict the lattice impact response. The following conclusions were made:

- The additive manufacturing stainless steel 316L was properly characterized under a quasi-static and dynamic regimen, with the properties summarized in Table. 2.
- The explicit-FE model developed predicted the Schwarz-diamond lattice response under quasi-static and dynamic regimen, with an average deviation of 5.25% in the plateau stress level and energy absorbed obtained from the experimental impact test.
- The FE model developed was to capture changes in the strain-stress response of graded and non-grades TPMS lattices.

References

[1] H. Jiang, H. Ziegler, Z. Zhang, H. Meng, D. Chronopoulos, and Y. Chen, "Mechanical properties of 3D printed architected polymer foams under large deformation," *Mater. Des.*, vol. 194, p. 108946, 2020, doi: 10.1016/j.matdes.2020.108946.

[2] S. L. Lu, M. Qian, H. P. Tang, M. Yan, J. Wang, and D. H. StJohn, "Massive transformation in Ti-6Al-4V additively manufactured by selective electron beam melting," *Acta Mater.*, vol. 104, pp. 303–311, 2016, doi: 10.1016/j.actamat.2015.11.011.

[3] T. Tancogne-Dejean, X. Li, M. Diamantopoulou, C. C. Roth, and D. Mohr, "High Strain Rate Response of Additively-Manufactured Plate-Lattices: Experiments and Modeling," *J. Dyn. Behav. Mater.*, vol. 5, no. 3, pp. 361–375, 2019, doi: 10.1007/s40870-019-00219-6.

[4] C. Bonatti and D. Mohr, "Mechanical performance of additively-manufactured anisotropic and isotropic smooth shell-lattice materials: Simulations & experiments," *J. Mech. Phys. Solids*, vol. 122, pp. 1–26, Jan. 2019, doi: 10.1016/j.jmps.2018.08.022.

[5] D. W. Abueidda, A. S. Dalaq, R. K. Abu Al-Rub, and H. A. Younes, "Finite element predictions of effective multifunctional properties of interpenetrating phase composites with novel triply periodic solid shell architectured reinforcements," *Int. J. Mech. Sci.*, vol. 92, pp. 80–89, Mar. 2015, doi: 10.1016/j.ijmecsci.2014.12.004.

[6] A. S. Dalaq, D. W. Abueidda, R. K. Abu Al-Rub, and I. M. Jasiuk, "Finite element prediction of effective elastic properties of interpenetrating phase composites with architectured 3D sheet reinforcements," *Int. J. Solids Struct.*, vol. 83, pp. 169–182, Apr. 2016, doi: 10.1016/j.ijsolstr.2016.01.011.

[7] A. S. Dalaq, D. W. Abueidda, and R. K. Abu Al-Rub, "Mechanical properties of 3D printed interpenetrating phase composites with novel architectured 3D solid-sheet reinforcements," *Compos. Part A Appl. Sci. Manuf.*, vol. 84, pp. 266–280, May 2016, doi: 10.1016/j.compositesa.2016.02.009.

[8] D. W. Lee, K. A. Khan, and R. K. Abu Al-Rub, "Stiffness and yield strength of architectured foams based on the Schwarz Primitive triply periodic minimal surface," *Int. J. Plast.*, vol. 95, pp. 1–20, 2017, doi: 10.1016/j.ijplas.2017.03.005.

[9] O. Al-Ketan, R. Rowshan, and R. K. Abu Al-Rub, "Topology-mechanical property

relationship of 3D printed strut, skeletal, and sheet based periodic metallic cellular materials," *Addit. Manuf.*, vol. 19, pp. 167–183, 2018, doi: 10.1016/j.addma.2017.12.006.

[10] F. S. L. Bobbert *et al.*, "Additively manufactured metallic porous biomaterials based on minimal surfaces: A unique combination of topological, mechanical, and mass transport properties," *Acta Biomater.*, vol. 53, pp. 572–584, Apr. 2017, doi: 10.1016/j.actbio.2017.02.024.

[11] O. Al-Ketan, R. Rowshan, A. N. Palazotto, and R. K. Abu Al-Rub, "On Mechanical Properties of Cellular Steel Solids with Shell-Like Periodic Architectures Fabricated by Selective Laser Sintering," *J. Eng. Mater. Technol. Trans. ASME*, vol. 141, no. 2, pp. 1–12, 2019, doi: 10.1115/1.4041874.

[12] N. Novak *et al.*, "Quasi-static and dynamic compressive behaviour of sheet TPMS cellular structures," *Compos. Struct.*, vol. 266, no. September 2020, pp. 1–10, 2021, doi: 10.1016/j.compstruct.2021.113801.

[13] H. Kuhn and D. Medlin, Eds., *Mechanical Testing and Evaluation*. ASM International, 2000.

[14] W. Chen and B. Song, *Split Hopkinson (Kolsky) Bar*. Boston, MA: Springer US, 2011.

[15] M. A. Kariem *et al.*, "Round-Robin test of split Hopkinson pressure bar," *Int. J. Impact Eng.*, vol. 126, pp. 62–75, Apr. 2019, doi: 10.1016/j.ijimpeng.2018.12.003.

[16] ASTM E8, "ASTM E8/E8M standard test methods for tension testing of metallic materials 1," *Annu. B. ASTM Stand. 4*, no. C, pp. 1–27, 2010, doi: 10.1520/E0008.